



OPEN

Spatial confinement affects the heterogeneity and interactions between shoaling fish

Gabriel Kuntz¹, Junxiang Huang², Mitchell Rask¹, Alex Lindgren-Ruby¹, Jacob Y. Shinsato¹, Dapeng Bi² & A. Pasha Tabatabai^{1,3}✉

Living objects are able to consume chemical energy and process information independently from others. However, living objects can coordinate to form ordered groups such as schools of fish. This work considers these complex groups as living materials and presents imaging-based experiments of laboratory schools of fish to understand how activity, which is a non-equilibrium feature, affects the structure and dynamics of a group. We use spatial confinement to control the motion and structure of fish within quasi-2D shoals of fish and use image analysis techniques to make quantitative observations of the structures, their spatial heterogeneity, and their temporal fluctuations. Furthermore, we utilize Monte Carlo simulations to replicate the experimentally observed data which provides insight into the effective interactions between fish and confirms the presence of a confinement-based behavioral preference transition. In addition, unlike in short-range interacting systems, here structural heterogeneity and dynamic activities are positively correlated as a result of complex interplay between spatial arrangement and behavioral dynamics in fish collectives.

Nature provides fantastic examples of complex collective behaviors on many length scales in order to accomplish certain tasks. For example, cells within tissues coordinate to successfully close wounds^{1,2}, ants build structures to overcome obstacles^{3,4}, and fish form cohesive groups to improve computations about their environment^{5,6}. In each of these examples, the interactions between individuals lead to function on a larger scale.

Understanding the details of the interactions between individuals within these complex groups is an active area of research^{7,8}. Previously, it has been shown that metric interactions, where constituents within a certain distance interact, qualitatively capture the collective behaviors seen in flocking⁹. However, closer inspections in a variety of species suggest that the true interactions are more likely visual, topological^{10–12}, or more complicated¹³. The pursuit of understanding these interactions is valuable to understanding fundamental problems in complex systems.

However, this connection between constituent interactions and bulk behavior parallels the language used to describe and design materials. Examples of this include tuning the interaction strength between colloids to influence colloidal gel rheology^{14–17}, the interaction specificity within DNA hybridized colloids and material structure^{18–20}, and the relative physical parameters within models of epithelial tissue and tissue fluidity^{21,22}. Therefore, this search for the relationship between interactions and bulk behavior is also critical for defining collective systems as living materials in-and-of themselves. In particular, these living materials are fundamentally non-equilibrium due to the local consumption of energy by each entity, and definitions of the mechanical^{23–25} or thermodynamic^{26,27} properties of these systems will help determine the material possibilities of these types of systems.

In this paper, we aim to understand the mechanical properties of a quasi-2D living material - groups of aquarium fish within the lab; for simplicity, we confine fish to thin volumes of water. We make quantitative observations of groups of swimming fish using image analysis techniques to identify fish positions and trajectories. We track fluctuations of structures at the local and group level as self-generated deformations. We find that we can control the motile behaviors of these fish by varying the level of spatial confinement and that this change in individual motion is correlated with a changing heterogeneity of the group. In addition, we employ Monte Carlo simulations to recreate the complex dynamics of fish interactions and examine the effects of varying spatial constraints on the group's mechanical properties. By using simulations to replicate experimentally measured distributions, we infer effective interactions between individuals. Through a wide variety of metrics, we

¹Department of Physics, Seattle University, Seattle, WA 98122, USA. ²Department of Physics, Northeastern University, Boston, MA 02115, USA. ³Physics Department, California Polytechnic State University, San Luis Obispo, CA 93410, USA. ✉email: pashatab@calpoly.edu

observe a behavioral transition as a function of spatial confinement which correlates with changes in structural heterogeneity. In contrast to colloidal gels involving short-range interactions, the simulations uncover a positive correlation between structural heterogeneity and dynamic activities.

Results

Cardinal tetra fish are imaged moving freely within quasi-2D cylindrical arenas with a depth of 1.5 ± 0.1 cm (“Methods”). Fish positions \mathbf{r} are identified using the open-source software TRex²⁸ which identifies fish body cross-sections through image contrast. We also use this software to connect fish positions in time to build trajectories $\mathbf{r}(t)$ and calculate instantaneous velocities $\mathbf{v}(t)$ for each fish (Methods). Since we now have the projected area of each fish, we use the mid-line length to characterize fish size. We find fish have a length of $L = 2.0 \pm 0.2$ cm (mean \pm stdev) (Fig. 1).

We record videos of 25 fish within arenas of different radii (R) to investigate the effects of confinement (Fig. 2a); these hard boundaries are not necessarily equivalent to the ‘soft’ boundaries generated by light patterning²⁹. Altering the radius R adjusts the global area density $\rho_g = N/(\pi R^2)$. However, it is crucial to note that fish can exhibit significant local density fluctuations since they do not uniformly occupy the entire space^{30,31}. We observe that arena size influences the probability distribution of speeds (v), where decreasing R biases the distributions towards slower speeds (Fig. 2b). This broad distribution of speeds is consistent with the stop-start motion associated with fish motility³². We fit each speed probability distribution to a modified Rayleigh distribution.

$$P(v) = \frac{v + b}{a} e^{-(v+b)^2/(2a)} \quad (1)$$

where a and b are fitting parameters associated with the width and shift of the distribution accordingly. We find that both of these parameters increase with R (Fig. 2c). This functional form was chosen to resemble the 2D Maxwell-Boltzmann distribution in an attempt to make parallels between the motion of molecules at thermodynamic equilibrium and the motion of fish out-of-equilibrium; this connection is discussed further in the “Discussion” section.

While Fig. 2b indicates that the extent of motion is affected by R , it does not describe the persistence of motion. As such, we calculate the mean squared displacement (MSD)

$$MSD(\tau) = \langle (\mathbf{r}(t + \tau) - \mathbf{r}(t))^2 \rangle \quad (2)$$

by comparing positions $\mathbf{r}(t)$ as a function of elapsed time (τ) for each fish; we average the MSD from all fish within an experiment to generate a single ensemble-averaged MSD (Fig. 2d, “Methods”). For large τ , the MSD turnover and plateau are set by the finite size of the arena. For small τ , we observe power-law scaling (i.e.

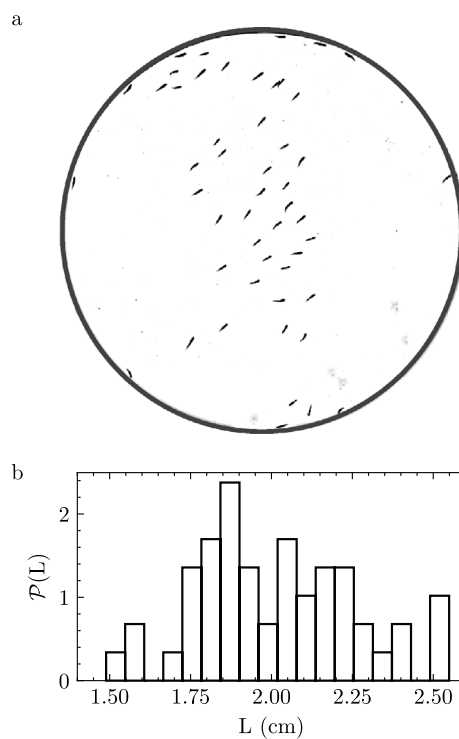


Figure 1. (a) Image of 50 fish within arena with radius $R = 44.25$ cm. Arena boundary outlined for clarity. (b) Probability distribution of fish mid-line length (L) for 50 fish in (a).

a

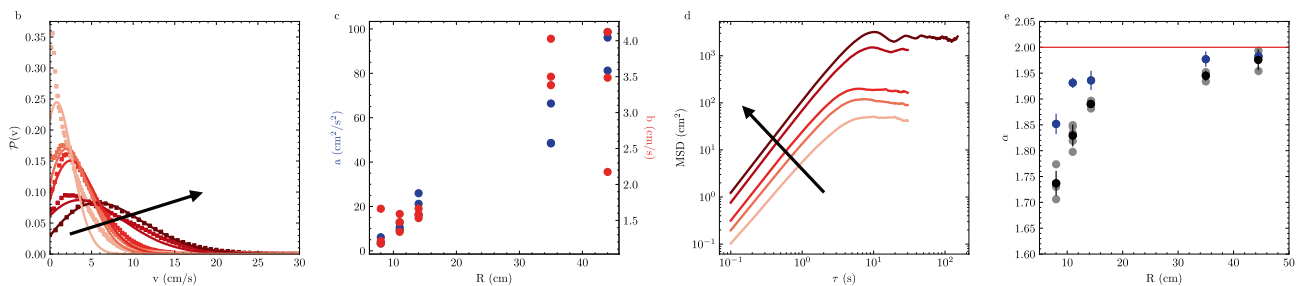
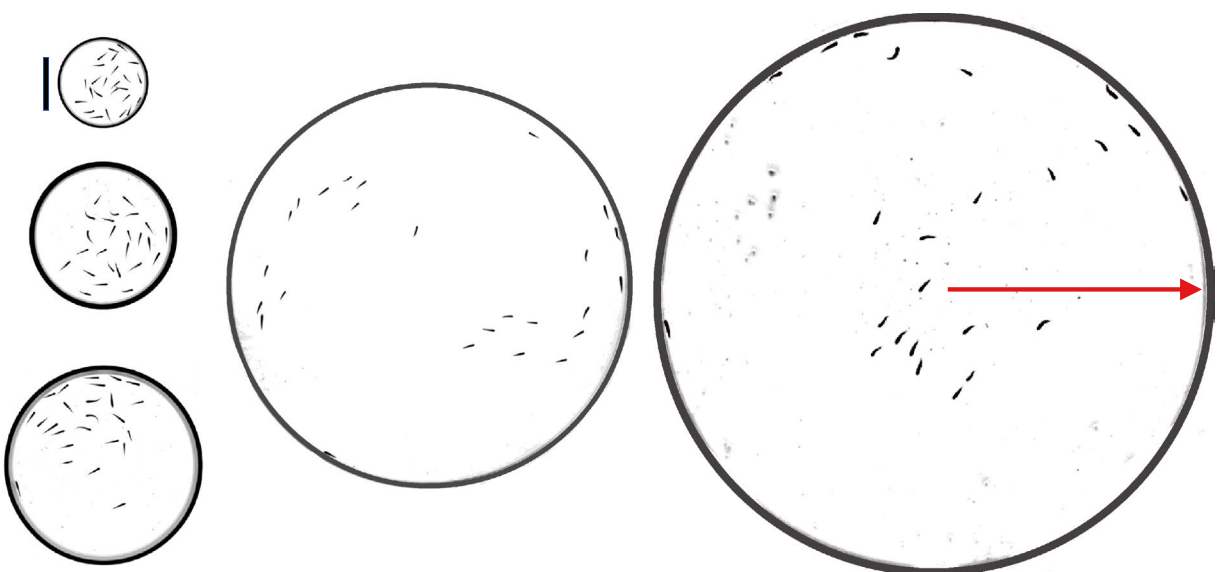


Figure 2. Confinement affects motion. (a) Images of arenas with radii $R = 8$ cm, 11 cm, 14 cm, 34.25 cm and 44.25 cm containing 25 fish. Arena boundaries were added for clarity. The red arrow denotes radius R . The scale bar is 10 cm. (b) Example probability distributions of fish speed (v) for 25 fish in the differently sized arenas (markers) and best fit Rayleigh distributions (lines). (c) Fitting parameters a (left-blue) and b (right-red) for fits to $P(v)$. (d) Mean squared displacement (MSD) as a function of elapsed time (τ) for fish in five different arenas. (e) The short-time power-law slope of MSD (α) as a function of radii (R). Experimental duplicates of α are plotted in grey ($N = 3$ for each), with the mean plotted in black. α for the shoal center of mass motion (blue, $N = 3$ for each). Error bars are one standard deviation. R increases along the arrows in (b,d).

$MSD \sim \tau^\alpha$ where α characterizes the type of motion. We find that α depends on confinement, demonstrating that fish motion is super-diffusive ($1 < \alpha < 2$) and approaches ballistic motion ($\alpha \rightarrow 2$) as containers get larger (Fig. 2e). The MSD of the shoal's center of mass has similar arena-size dependent values of α (Fig. 2e, Supplemental Fig. 1).

We next asked how these differences in motion affected the organization of fish in groups. To investigate the effects of confinement on structural and material properties of the shoal we use fish positions $\mathbf{r}(t)$ to calculate the time-varying convex hull (Fig. 3a, “Methods”) which we use to define the overall geometric size of the group. The area of the convex hull A_H fluctuates considerably over time, signifying that the group is exploring different fractions of the space (Fig. 3b). While A_H fluctuates in time, the time-averaged fraction of space occupied by the shoal $\langle A_H \rangle / \pi R^2$ is consistent across different confinements (Fig. 3c); on average, the shoal will fill the space to an equal extent regardless of the amount of space it has available to it (Supplemental Fig. 2).

The size of a shoal characterized by A_H is prone to bias by fish that do not move with the group. Therefore, we define a local measurement of the space occupied by individual fish by calculating the Voronoi tessellation using the fish positions \mathbf{r} . The Voronoi cell for a particular fish is the space that is most proximal to a fish; this acts as an amorphous unit cell. We restrict our structural analysis at each frame to fish that have Voronoi cells completely enclosed within the convex hull (Fig. 4a); these ‘internal’ fish have Voronoi areas which are both closed and do not drastically change with small neighbor movements. We calculate the areas of each of these Voronoi cells A for individual fish and find that they fluctuate through time as well. In Fig. 4b, we show an example Voronoi area that fluctuates by an order of magnitude in area over the plotted observation window. We also note that the data point frequency is not constant over the observation window; no Voronoi area is calculated for this fish if it fails to be an ‘internal’ fish or if we cannot uniquely identify all fish in a particular frame.

The number of these internal fish N_{int} varies widely over time (Fig. 4c inset) and each internal fish has an average of approximately six topological neighbors, defined as neighbors that share a Voronoi edge (Supplemental Fig. 3). Therefore, to further understand the relationship between local fluctuations in A and shoal level

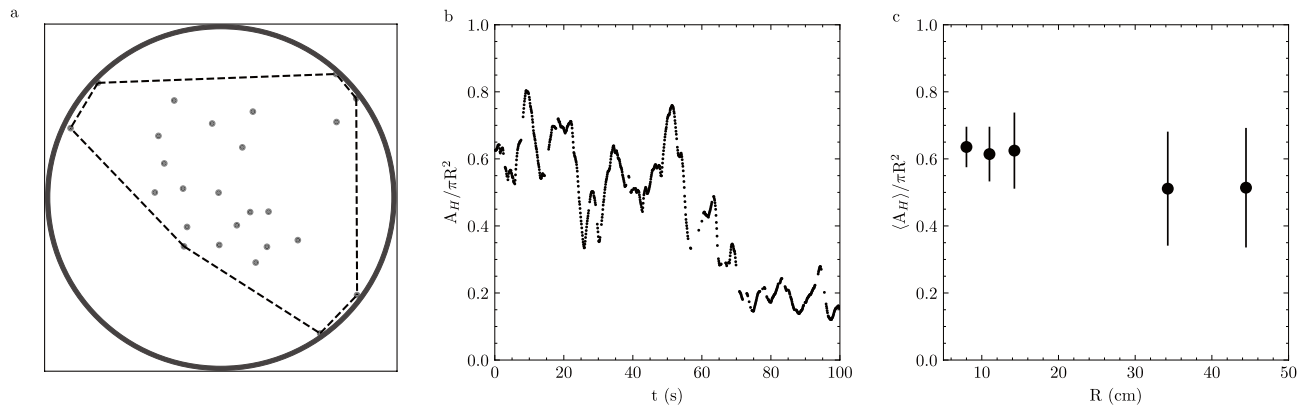


Figure 3. Shoal area fluctuates in time. (a) Convex hull of 25 fish in $R = 44.25$ cm arena. Fish positions are grey markers. Convex hull is defined by the black dashed line. The image width is $2R$ with the arena boundary outlined for clarity. (b) Example of convex hull area (A_H) normalized to arena area (πR^2) as a function of time for 25 fish in $R=34.25$ cm arena. (c) Time average convex hull area ($\langle A_H \rangle$) normalized by arena area for arenas of different radii. Error bars are one standard deviation.

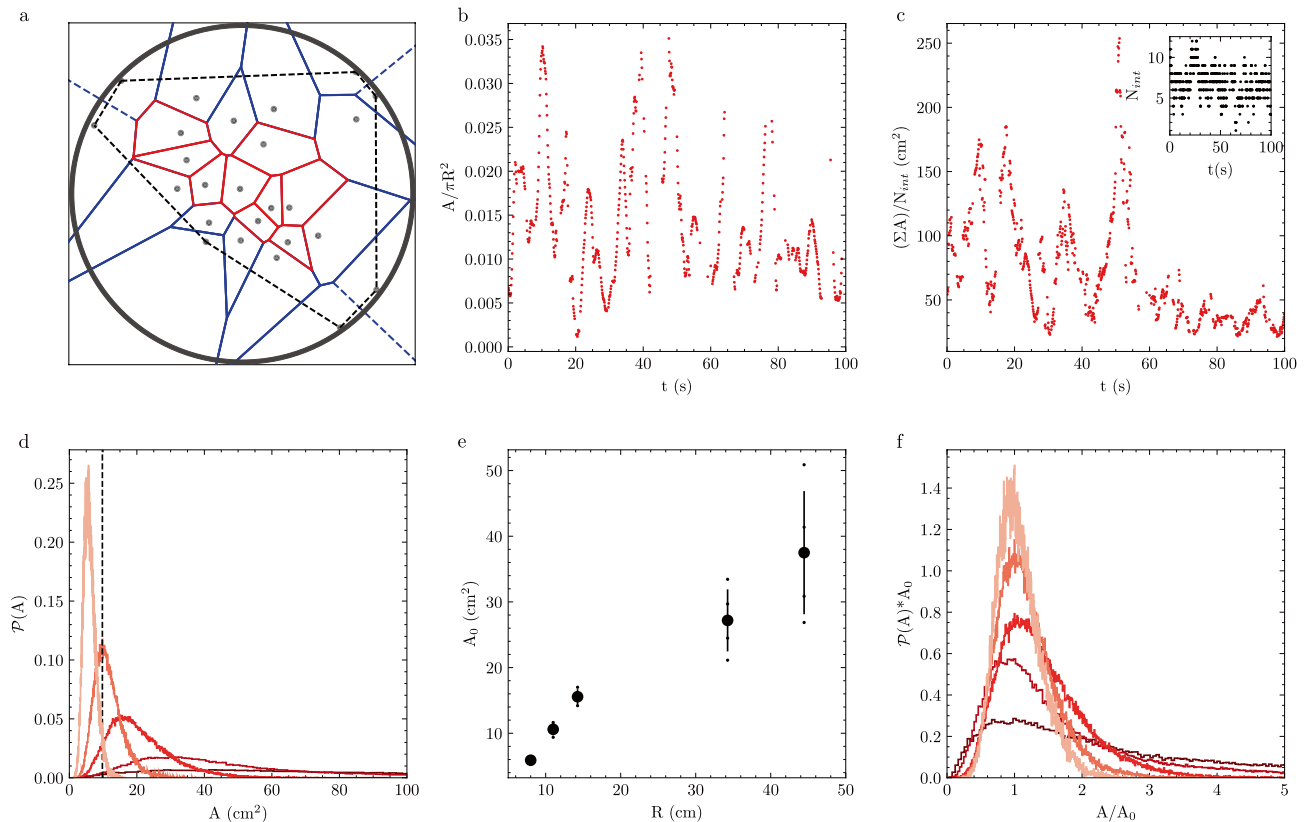


Figure 4. Confinement affects local fish packing. (a) Voronoi tessellation (polygons) of 25 fish (grey markers) in $R = 44.25$ cm arena. Internal fish (red polygons) are a subset of all fish and have all vertices within the convex hull (black dashed line). The image width is $2R$ with the arena boundary outlined for clarity. (b) Example time evolution of a single fish Voronoi area (A) normalized by arena area (πR^2) in $R = 34.25$ cm arena. (c) Sum of internal areas (ΣA) normalized by number of internal fish (N_{int}) as a function of time for data in (b). (c-inset) Number of internal fish (N_{int}) as a function of time for data in (b). (d) Probability distributions ($P(A)$) of internal areas (A) for 25 fish for different arena sizes. The vertical dashed line indicates the peak of a distribution A_0 . (e) A_0 as a function of arena radii (R). Bold circles are averages across different fish groups, small data points are individual experiments and error bars are one standard deviation. (f) Scaled probability distributions from (d). Colors in (d,f) darken with increasing R .

fluctuations, we estimate the time-varying net size of all internal fish $\sum A/N_{int}$ (Fig. 4c). We note that the time courses of the A_H (Fig. 3b), A (Fig. 4b), and $\sum A/N_{int}$ (Fig. 4c) all come from the same experiment and are plotted over the same range of time. The relative size of fluctuations within A_H and $\sum A/N_{int}$ are qualitatively similar. However, these are not equivalent to the fluctuations of A over the same time period. Therefore, the group and the individual area fluctuations are not mirrored, and fish areas do not all uniformly expand or shrink collectively.

Since shoals occupy larger spaces in larger arenas (Fig. 4c), the Voronoi region associated with each fish must also vary with R . Indeed, we see this dependence in the probability distributions of A for all internal fish within an experiment, where increasing R biases the distribution to larger areas A (Fig. 4d). We define the modal area A_0 as the peak of the distribution which increases with arena size, however, it does not increase $\sim R^2$ as would be expected for a 2D gas (Fig. 4e).

By comparing the normalized probability distributions ($P(A) * A_0$ vs A/A_0), we show that the fluctuations observed are statistically similar between small arena sizes yet vary significantly for larger arenas (Fig. 4f); this is consistent with the arena size dependence of MSD scaling in Fig. 2. We also show that these distributions are not equivalent to distributions made from randomly generated points, consistent with the fact that fish are not randomly occupying space (Supplemental Fig. 4).

Upon inspection, the probability distribution of observed internal Voronoi areas is not symmetric about the mode A_0 (Fig. 5a). Here, we take an approach that is similar to the computational modeling of cells in tissues via the Vertex and Self-Propelled Voronoi models where deviations of a cell from a modal area are associated with an energy cost for that cell^{21,22}. To understand the underlying dynamics that result in the asymmetric distributions in Fig. 4d, we fit two separate parabolic functions to each distribution such that

$$P(A_0) - P(A) \sim \begin{cases} k_c(A - A_0)^2, & \text{if } A < A_0 \\ k_e(A - A_0)^2, & \text{if } A > A_0 \end{cases} \quad (3)$$

with constants k_c and k_e associated with compression and expansion, respectively, of Voronoi areas away from the modal area A_0 (Fig. 5a, “Methods”). The ratio k_e/k_c of these constants is a signature of the effective interactions between fish, which varies with R (Fig. 5b).

Simulations

Previous literature has established that the area distribution of cells within two-dimensional random Voronoi networks adheres to a Gamma distribution³³. The probability density function (PDF) for such a distribution is mathematically represented as:

$$f_\Gamma(x) = \frac{x^{k-1} e^{-x/\theta}}{\theta^k \Gamma(k)}, \quad (4)$$

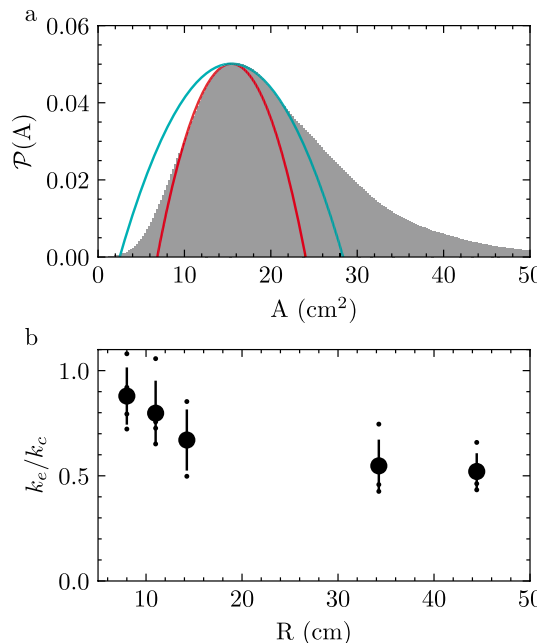


Figure 5. Confinement affects area distribution asymmetry. (a) Example probability distribution of internal fish voronoi areas (A) for $R = 14$ cm arena (143,963 instances). Parabolic fits to $A < A_0$ (red) and $A > A_0$ (cyan) associated with compression and expansion, respectively. (b) Ratio of coefficients of expansion k_e and compression k_c found from fit in (a) as a function of arena radius (R). Small markers are individual experiments, and the large black markers are the mean with one standard deviation error bar.

where k and θ are the shape and scale parameters, respectively, while $\Gamma(*)$ denotes the gamma function. For random Voronoi networks, a shape parameter $k = 3.63$ is reported to yield the best fit to the observed cell area distribution³⁴. In addition, for hard disks, the distribution of Voronoi free area, which is the difference between the actual Voronoi cell area and the minimum cell area at close packing, is well described by a Gamma distribution with k between 3 to 4³⁵.

Intriguingly, despite the non-equilibrium and non-random nature of the fish collective, the internal area distributions at smaller radii R conform closely to a Gamma distribution (Fig. 6a–c). The shape parameter k , which governs the distribution asymmetry and tail behavior, is greater than the non-interacting limit ($k = 3.6$). Large k values represent a more symmetric bell-shaped curve indicative of low heterogeneity and a tendency for cell areas to aggregate around the mean. This pattern suggests that interactions between fish within small arenas lead to a more homogeneous structural arrangement; this reduces variability and allows each fish to navigate and occupy space more effectively. As the arena radius R increases, there is a clear increase in the Voronoi area heterogeneity with two distinct signatures: a decrease in the k value and the emergence of an exponential tail in the distribution (Fig. 6d–f). At large arenas such as $R = 34.25$ cm or 44.25 cm, the internal areas initially adhere to a Gamma distribution up to a threshold around $1.5A_0$. Beyond this point, the distribution exhibits strong exponential tails indicative of highly heterogeneous shoal structure and significant probabilities of finding large cells and large local density fluctuations. This phenomenon bears resemblance to the behavior observed in granular aggregates with capillary interactions, while the fish shoal is unique in its ability to adapt the k value, which is obtained by fitting the bulk of the distribution to a Gamma distribution and is observed to change across a broad range³⁶.

The structural heterogeneity and dynamics are frequently interlinked. In colloidal gels formed through short-range attractive interactions, an increase in interaction strength leads to an increase in structural heterogeneity and dynamical arrest^{37,38}. However, our observations in fish collectives present a contrasting scenario. Due to the long-range nature of their interactions, both structural heterogeneity and dynamical activities escalate with a larger radius R . In these larger arenas, local densities experience more pronounced fluctuations which result in varied behavioral patterns: some fish form tightly-knit compact shoals while others simultaneously and independently navigate the container.

To elucidate the influence of the arena radius on fish interactions and the interplay between heterogeneity and dynamical activities, we implement a Monte Carlo model that simulates the fish positions with different arena radii and $\beta = 1/k_B T$. At each simulation step n , we randomly select a fish, indexed as i , and propose its

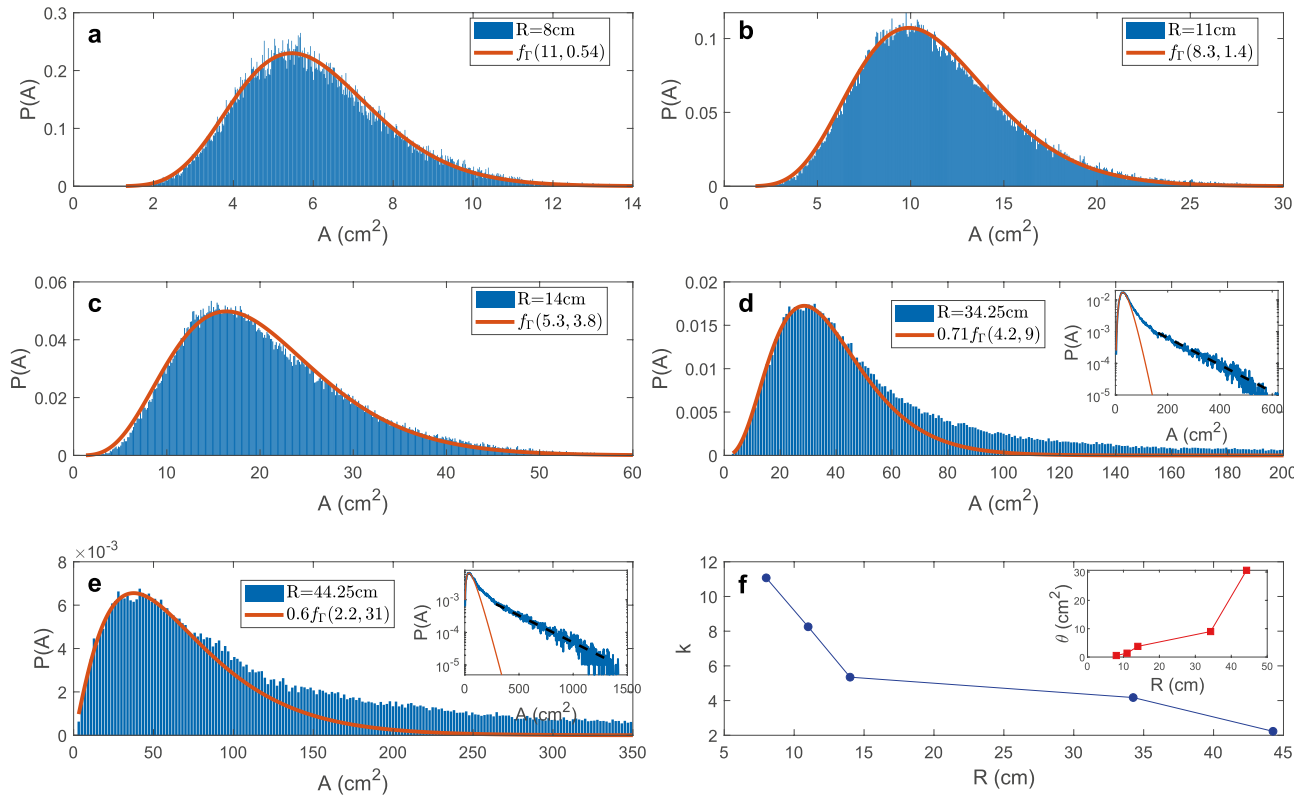


Figure 6. The heterogeneity of internal Voronoi areas increases as the density is decreased. (a–e) Experimental area A distributions are fit to Gamma distribution (red) for $R = 8, 11, 14, 34.25$ and 44.25 cm radii arenas. $f_\Gamma(k, \theta)$ denotes the PDF of Gamma distribution defined in Eq. (4). (d,e) At $R = 34.25$ cm and 44.25 cm the Gamma distribution fit is done for $A < 1.5A_0$ and a normalization factor is applied to $f_\Gamma(k, \theta)$ to align the modes. Insets in (d,e) show exponential tails (black dashed lines) with decay parameters of 0.0098 and 0.0038 cm^{-2} , respectively. (f) The shape parameter k as a function of arena radii R . (f-inset) The scale parameter θ as a function of arena radii R .

subsequent position as $X_{i,n+1} = X_{i,n} + \sigma \delta X_{i,n}$, where $X_{i,n}$ represents the position of fish i at step n , σ is the step size, and $\delta X_{i,n}$ is Gaussian white noise with unit variance. The Morse potential is adapted to emulate the complex dynamics of fish schooling by treating the interactions between fish as attractive and repulsive inter-fish forces. The potential is expressed as

$$U(r) = (1 - e^{1-r/r_0})^2, \quad (5)$$

where r is the actual distance between two fish, and r_0 is the preferred distance. A proposed move that results in an energy change ΔE is accepted with probability $\min(1, e^{-\beta \Delta E})$. We conducted the simulation with a step size $\sigma = 0.4$ over 10^7 iterations, recording the internal area metrics every 100 steps. β approaching zero would correspond to the ideal gas limit where the interaction between fish vanishes. To find out the parameters that best describe the experiments, we systematically sweep the parameter space of r_0 ranging from 0.1 to 20 and β ranging from 0 to 2 for different simulations. The resulting area distributions are then statistically analyzed using the chi-squared method to determine the optimal values for r_0 and β corresponding to each radius R . Despite this simplicity of this model, the Monte Carlo simulations successfully reproduce the experimentally observed area distributions (Fig. 7a–c). This indicates that the core principles and rules embedded in the Monte Carlo model are effective in capturing the essential dynamics of fish interactions.

Interestingly, the preferred distance r_0 and β display a non-monotonic variation as a function of R , with a transition point located between $R = 14$ cm and 34.25 cm (Fig. 7d). This non-monotonic variation suggests a complex interplay between individual space requirements and the benefits of social interactions. In small arenas, the high density compels fish to maintain a small r_0 . When more space is available, fish tend to increase their preferred distance r_0 to avoid overcrowding and reduce stress, with a decreasing β indicative of increased activities. With sufficient space, however, behavior changes and a decrease in r_0 imply a shift toward preserving the advantages of schooling such as enhanced communication and collective vigilance. Such a transition explains the dramatic decrease of A_0/R^2 for the big radii in Fig. 4e, in contrast to a constant ratio in the non-interacting limit or $\beta = 0$. The presence of a transition point indicates a threshold at which the fish alter their spacing behavior, possibly to balance the conflicting needs for individual space and group affiliation as a strategic response to maximize the evolutionary benefits of schooling.

Discussion

In this manuscript, we have treated a quasi-2D shoal of fish as a living material, and we have demonstrated the ability to control the average motion of individuals as well as the structures present within the group simply by changing the extent of confinement while keeping the number of individuals within the group constant.

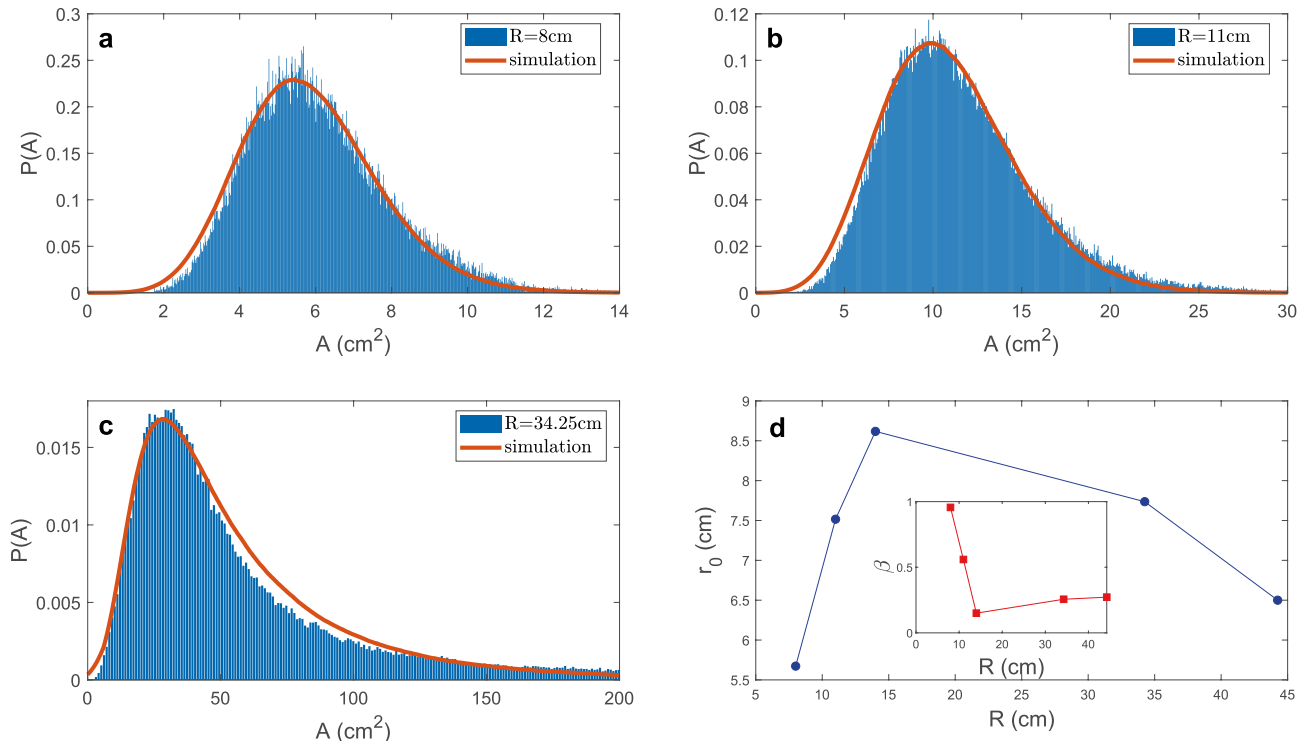


Figure 7. Interaction strength and length scale are influenced by confinement. (a–c) Sample comparisons between experimental internal area distributions A and Monte Carlo simulation (red line) for radii $R = 8\text{ cm}$, 11 cm , and 34.25 cm . (d) The preferred distance r_0 and (d-inset) parameter β as a function of arena radii R from Monte Carlo simulations.

In addition to this control of motion and structure, we argue below that (1) this control extends to the energy usage of fish while swimming as well as the effective energy of interaction between fish, (2) the inferred interactions are non-monotonic suggesting an induced behavioral change, (3) asymmetries in distributions of structure indicate asymmetries of local interactions, and 4) this shoal, while non-equilibrium in nature, shares a similarity with the ideal gas.

First, in describing the distribution of speeds in Fig. 2, we found that a Rayleigh function (Eq. 1) described our data well; this is reminiscent of a 2D Maxwell–Boltzmann distribution. To make this analogy, we consider the traditional Maxwell–Boltzmann distribution which describes the speed v of molecules with mass m of a gas at a given temperature T . In this form, $k_B T$ is the thermal energy scale where k_B is the Boltzmann constant. If we consider that $a = k_B T/m$ and that b is a fitting parameter for an offset speed in Eq. (1), then a is analogous to the amount of energy inputted. Traditionally this energy would be via thermal fluctuations per particle, however, a is not thermal in origin. Instead, this energy input comes from the energy usage of the fish towards swimming and is therefore a measure of non-equilibrium activity. This trend of the effective energy changing with confinement is also observed through the interaction energy within Monte Carlo simulations, where $\beta(R)$ in Fig. 7d is similar to $1/a$ in Fig. 2c.

Second, both the effective interaction length scale r_0 and energy scale β which are inferred through Monte Carlo simulations exhibit non-monotonic behaviors (Fig. 7d). This indicates that external confinement affects a transition where fish behavior changes as the arena increases size.

Third, we observe a decoupling of the local fluctuations in fish areas with the group level fluctuations in size, indicating that expansions and contractions of the group are not homogeneously distributed amongst individuals (Figs. 3b, 4b, c). We find that the distribution of internal Voronoi areas is asymmetric about the mode (Fig. 5) and is robust to the method of measurement (Supplemental Figs. 5, 6, and 7). However, the area distribution of non-interacting cells within a two-dimensional random Voronoi networks follows a Gamma distribution with $k = 3.6$ ³⁴, which corresponds to $k_e/k_c \approx 0.55$ (Supplementary Materials). As such, deviations from this non-interacting result in Fig. 5b are a direct result of biased interactions between compression and expansion as a result of confinement that we believe may provide information about the mechanical properties of these living materials.

These changes are robust. We find that *all* changes in structure or dynamics occur between $R = 14$ cm and $R = 34.25$ cm: fish motion (Fig. 2e), modal Voronoi area (Fig. 4e), distributions of Voronoi areas (Fig. 4f), the shapes of these distributions (Figs. 5b, 6), and the inferred radii and energy of interaction between fish (Fig. 7). As such, we conclude that spatial confinement is a consistent method to control the dynamical and mechanical properties of this non-equilibrium material.

Fourth, we show here that this complicated non-equilibrium material shares a similarity with a classic equilibrium material—the ideal gas. We notice that the increase in non-equilibrium activity a with system size R is correlated with a decrease in global density ρ_g . This interpretation of Fig. 2b, c suggests that fish consume more energy while swimming in the larger arenas. This is similar to an ideal gas at constant pressure: gas molecules must have more thermal energy to maintain a constant pressure if there are fewer molecules.

In all, we have demonstrated that this non-traditional non-equilibrium material can be tuned simply by changing the degree of external confinement. It is our hope that this facile control and the simple parallels to equilibrium materials establish this as a useful tool to learn more about the mechanical properties of non-equilibrium materials in general.

Methods

Fish care

Cardinal tetra (*Paracheirodon axelrodi*) fish are purchased from the Aquarium Co-Op in Edmonds WA. Fish are housed in a ~ 50 gallon living aquarium at a maximum density of 1 fish/gallon. Lights are set to a 12h–12h day–night cycle; all experiments are done during the daytime setting. Water is kept at a temperature between 77° and 79°F. Water pH is monitored and adjusted around 7.2–7.4 and ammonia, nitrate, and nitrite levels are monitored using the API Freshwater Test Kit and kept at undetectable levels. Fish are fed once daily.

All experimental protocols were approved by an Institutional Animal Care and Use Committee. All methods were carried out in accordance with the Institutional Animal Care and Use Committee and follow ARRIVE guidelines.

Experimental details

A total of 60 fish were used in this study. For experimental observations, 25 fish are chosen at random from sets of 30–60 fish in all data except Fig. 1 where 50 fish were used. Randomization is done through the act of netting fish within the living aquarium. Cardinal tetra have low sexual dimorphism and therefore the relative population of males and females within each experiment is also random. Experiments are repeated with new subsets of fish on different days.

The fish are transferred to shallow cylindrical arenas made for experiments. The temperature of the observation tank is kept between 77° and 79°F and the water used for this tank is directly taken from the living aquarium. The water depth is kept at 1.5cm with a tolerance of ± 0.1 cm across the arena. This minimizes 3D fish crossings that affect our fish identification algorithm. Arenas are made from either custom acrylic or white PVC. Clear acrylic arenas are lined with white tape to match PVC. Arena sizes are radii $R = 8$ cm, 11 cm, 14 cm, 34.25 cm, and 44.25 cm.

Shallow arenas are submerged in a large ~ 200 gallon water bath with active heating and water circulation which acts as a thermal reservoir but avoids generating any flow in the observation arenas. Water within the shallow container containing the fish is static except when perturbed by the fish within the observation arenas. Fish

are left undisturbed in the imaging arena for a minimum of one hour before imaging for acclimatization. Fish that do not move during this one hour period are replaced prior to experimental observation. No data are excluded.

Room lights are turned off and the room is vacated during video captures. Fish are back-lit by submerged broadband visible light. A diffusive acrylic layer separates the light source and the imaging aquarium base which helps to homogeneously illuminate the field of view. Room lights are turned off during acclimatization and experiments. Videos are recorded from overhead with a Pixelink PL-D7620 machine vision camera at 10 frames per second for up to 60 minutes. All probability distributions contain a minimum of 100,000 values. Data summaries in Fig. 2e are averages of three separate experiments for every arena radius. Data summaries in Figs. 3c and 4e are averages of three separate experiments ($R = 11, R = 14$ cm) and four separate experiments ($R = 8, R = 34.25, R = 44.25$ cm). Data summaries in Fig. 5b are averages of four separate experiments for every arena radius.

Image analysis

Videos are taken with lighting optimized to ensure shadows, bubbles, and any other visual noise are minimized before using the open-source software TRex²⁸ to threshold the videos and determine position, velocity, and orientation for individual fish. The pixel-to-centimeter conversion is found by taking a photograph of a ruler at the bottom of the arena after each experiment without disturbing the camera setup.

MSD analysis

The mean-squared-displacement MSD is calculated for each fish and averaged for all fish in an experiment. When we lose continuity in fish trajectories due to tracking errors, we ensure that the MSD is only calculated for consecutively tracked frames. The average consecutive track lengths for any given fish range from 59 s in the largest $R = 44.25$ cm arena to 18.8 s in the smallest $R = 8$ cm arena. Scaling exponent α is calculated via a power-law fit for $\tau \leq 1$ s.

Fitting area distributions

Two parabolas are fit to a probability distribution smoothed with a Gaussian filter and forced through a common peak A_0 in data such as Fig. 5a. Each parabola is either fit to values less than A_0 for compression or greater than A_0 for expansion. The range of values around A_0 that the parabolas are fit to be the same for both and is defined separately for each experiment. This range falls between 1/3 to 2/3 the value of A_0 .

Data availability

Datasets used and analyzed during the current study are available from the corresponding author on reasonable request.

Received: 19 January 2024; Accepted: 27 May 2024

Published online: 29 May 2024

References

1. Ajeti, V. *et al.* Wound healing coordinates actin architectures to regulate mechanical work. *Nat. Phys.* **15**(7), 696–705 (2019).
2. Brugués, A. *et al.* Forces driving epithelial wound healing. *Nat. Phys.* **10**(9), 683–690 (2014).
3. Ko, H., Hadgu, M., Komilian, K. & David, L. H. Small fire ant rafts are unstable. *Phys. Rev. Fluids* **7**(9), 090501 (2022).
4. Graham, J. M., Kao, A. B., Wilhelm, D. A. & Garnier, S. Optimal construction of army ant living bridges. *J. Theor. Biol.* **435**, 184–198 (2017).
5. Berdahl, A., Torney, C. J., Ioannou, C. C., Faria, J. J. & Couzin, I. D. Emergent sensing of complex environments by mobile animal groups. *Science* **339**(6119), 574–576 (2013).
6. Hein, A. M. *et al.* The evolution of distributed sensing and collective computation in animal populations. *eLife* **4**, e10955 (2015).
7. Katz, Y., Tunstrom, K., Ioannou, C. C., Huepe, C. & Couzin, I. D. Inferring the structure and dynamics of interactions in schooling fish. *Proc. Natl. Acad. Sci.* **108**(46), 18720–18725 (2011).
8. Sridhar, V. H. *et al.* The geometry of decision-making in individuals and collectives. *Proc. Natl. Acad. Sci.* **118**(50), 21021 (2021).
9. Vicsek, T., Czirók, A., Ben-Jacob, E., Cohen, I. & Shochet, O. Novel type of phase transition in a system of self-driven particles. *Phys. Rev. Lett.* **75**(6), 1226–1229 (1995).
10. Ballerini, M. *et al.* Interaction ruling animal collective behavior depends on topological rather than metric distance: Evidence from a field study. *Proc. Natl. Acad. Sci.* **105**(4), 1232–1237 (2008).
11. Camperi, M., Cavagna, A., Giardina, I., Parisi, G. & Silvestri, E. Spatially balanced topological interaction grants optimal cohesion in flocking models. *Interface Focus* **2**(6), 715–725 (2012).
12. Kumar, V. & De, R. *Flocking: Influence of Metric Versus Topological Interactions*. arXiv:2109.10088 (2021).
13. Torney, C. J. *et al.* Inferring the rules of social interaction in migrating caribou. *Philos. Trans. R. Soc. B Biol. Sci.* **373**(1746), 20170385 (2018).
14. Shah, S. A., Chen, Y.-L., Schweizer, K. S. & Zukoski, C. F. Viscoelasticity and rheology of depletion flocculated gels and fluids. *J. Chem. Phys.* **119**(16), 8747–8760 (2003).
15. Lu, P. J. *et al.* Gelation of particles with short-range attraction. *Nature* **453**(7194), 499–503 (2008).
16. Hsiao, L. C., Newman, R. S., Glotzer, S. C. & Solomon, M. J. Role of isostaticity and load-bearing microstructure in the elasticity of yielded colloidal gels. *Proc. Natl. Acad. Sci.* **109**(40), 16029–16034 (2012).
17. Nabizadeh, M. & Jamali, S. Life and death of colloidal bonds control the rate-dependent rheology of gels. *Nat. Commun.* **12**(1), 4274 (2021).
18. Benjamin Rogers, W. & Crocker, J. C. Direct measurements of DNA-mediated colloidal interactions and their quantitative modeling. *Proc. Natl. Acad. Sci.* **108**(38), 15687–15692 (2011).
19. Wang, Yu. *et al.* Crystallization of DNA-coated colloids. *Nat. Commun.* **6**(1), 7253 (2015).
20. Hayakawa, D. *et al.* Geometrically programmed self-limited assembly of tubules using DNA origami colloids. *Proc. Natl. Acad. Sci.* **119**(43), e2207902119 (2022).
21. Dapeng, B., Lopez, J. H., Schwarz, J. M. & Lisa Manning, M. A density-independent rigidity transition in biological tissues. *Nat. Phys.* **11**(12), 1074–1079 (2015) (Number: 12 Publisher: Nature Publishing Group.).

22. Yang, X. *et al.* Correlating cell shape and cellular stress in motile confluent tissues. *Proc. Natl. Acad. Sci. USA* **114**(48), 12663–12668 (2017).
23. Lee, R. M., Kelley, D. H., Nordstrom, K. N., Ouellette, N. T. & Losert, W. Quantifying stretching and rearrangement in epithelial sheet migration. *New J. Phys.* **15**(2), 025036 (2013).
24. Ni, R., Puckett, J. G., Dufresne, E. R. & Ouellette, N. T. Intrinsic fluctuations and driven response of insect swarms. *Phys. Rev. Lett.* **115**(11), 118104 (2015).
25. van der Vaart, K., Sinhuber, M., Reynolds, A. M. & Ouellette, N. T. Mechanical spectroscopy of insect swarms. *Sci. Adv.* **5**(7), 9305 (2019).
26. Takatori, S. C., Yan, W. & Brady, J. F. Swim pressure: Stress generation in active matter. *Phys. Rev. Lett.* **113**(2), 028103 (2014).
27. Bowick, M.J., Nikta Fakhri, M., Marchetti, C. & Ramaswamy, S. *Symmetry, Thermodynamics and Topology in Active Matter*. arXiv: [2107.00724](https://arxiv.org/abs/2107.00724) (2021).
28. Walter, T. & Couzin, I.D. TRex, a fast multi-animal tracking system with markerless identification, and 2D estimation of posture and visual fields. *eLife* **10** (2021).
29. Giannini, J. A. & Puckett, J. G. Testing a thermodynamic approach to collective animal behavior in laboratory fish schools. *Phys. Rev. E* **101**(6), 062605 (2020).
30. Makris, N. C. *et al.* Fish population and behavior revealed by instantaneous continental shelf-scale imaging. *Science* **311**(5761), 660–663 (2006).
31. Becco, Ch., Vandewalle, N., Delcourt, J. & Poncin, P. Experimental evidences of a structural and dynamical transition in fish school. *Phys. A Stat. Mech. Appl.* **367**, 487–493 (2006).
32. Li, G., Kolomenskiy, D., Liu, H., Godoy-Diana, R. & Thiria, B. Intermittent versus continuous swimming: An optimization tale. *Phys. Rev. Fluids* **8**(1), 013101 (2023) (Publisher: American Physical Society).
33. Kiang, T. Random fragmentation in two and three dimensions. *Z. Astrophys.* **64**(433), 64:433 (1966).
34. Weaire, D., Kermode, J. P. & Wejchert, J. On the distribution of cell areas in a Voronoi network. *Philos. Mag. B* **53**(5), L101–L105 (1986).
35. Kumar, N., Soni, H., Ramaswamy, S. & Sood, A. K. Flocking at a distance in active granular matter. *Nat. Commun.* **5**(1), 4688 (2014).
36. Berhanu, M. & Kudrolli, A. Heterogeneous structure of granular aggregates with capillary interactions. *Phys. Rev. Lett.* **105**(9), 098002 (2010).
37. Dibble, C. J., Kogan, M. & Solomon, M. J. Structure and dynamics of colloidal depletion gels: Coincidence of transitions and heterogeneity. *Phys. Rev. E* **74**(4), 041403 (2006).
38. Hsiao, L. C. *et al.* Metastable orientational order of colloidal discoids. *Nat. Commun.* **6**(1), 8507 (2015).

Acknowledgements

APT was supported by the M.J. Murdock Charitable Trust Award Number FSU-201913717. APT, GK, MR, and JS were supported by the National Science Foundation Award Number 2137509. JH, DB, and APT were supported by National Science Foundation Award Number DMR-2046683.

Author contributions

GK and MR collected experimental data. GK, MR, and ALR contributed analytical tools. GK, JH, MR, and JS analyzed data. JH and DB conducted simulations. APT, GK, JH, DB, and MR wrote the manuscript. APT and GK edited the manuscript. APT designed and conceived the work.

Competing interests

The authors declare no competing interests.

Additional information

Supplementary Information The online version contains supplementary material available at <https://doi.org/10.1038/s41598-024-63245-y>.

Correspondence and requests for materials should be addressed to A.P.T.

Reprints and permissions information is available at www.nature.com/reprints.

Publisher's note Springer Nature remains neutral with regard to jurisdictional claims in published maps and institutional affiliations.



Open Access This article is licensed under a Creative Commons Attribution 4.0 International License, which permits use, sharing, adaptation, distribution and reproduction in any medium or format, as long as you give appropriate credit to the original author(s) and the source, provide a link to the Creative Commons licence, and indicate if changes were made. The images or other third party material in this article are included in the article's Creative Commons licence, unless indicated otherwise in a credit line to the material. If material is not included in the article's Creative Commons licence and your intended use is not permitted by statutory regulation or exceeds the permitted use, you will need to obtain permission directly from the copyright holder. To view a copy of this licence, visit <http://creativecommons.org/licenses/by/4.0/>.

© The Author(s) 2024